scientific reports

Check for updates

OPEN

Automated brain tumor recognition using equilibrium optimizer with deep learning approach on MRI images

Mahmoud Ragab[1]✉, Iyad Katib[2], Sanaa A. Sharaf[2], Hassan A. Alterazi[1], Alanoud Subahi[3], Sana G. Alattas[4], Sami Saeed Binyamin[5] & Jaber Alyami[6,7]

Brain tumours (BT) affect human health owing to their location. Artificial intelligence (AI) is intended to assist in diagnosing and treating complex diseases by combining technologies like deep learning (DL), big data analytics, and machine learning (ML). AI can identify and categorize tumours by analyzing brain imaging approaches like Magnetic Resonance Imaging (MRI). The medical sector has been promptly shifted by evolving technology, and an essential element of these transformations is AI technology. AI model determines tumours' class, size, aggressiveness, and location. This assists medical doctors in making more exact diagnoses and treatment plans and helps patients better understand their health. Also, AI is used to track the progress of patients through treatment. AI-based analytics is used to predict potential tumour recurrence and assess treatment response. This study presents Brain Tumor Recognition using an Equilibrium Optimizer with a Deep Learning Approach (BTR-EODLA) technique for MRI images. The BTR-EODLA technique intends to recognize whether or not a BT presence exists. In the BTR-EODLA technique, median filtering (MF) is deployed to eliminate the noise in the input MRI. Besides, the squeeze-excitation ResNet (SE-ResNet50) model is applied to derive feature vectors, and its parameters are fine-tuned by the design of the EO model. The BTR-EODLA technique utilizes the stacked autoencoder (SAE) model for BT detection. A sequence of experiments is performed to ensure the improved performance of the BTR-EODLA technique. The investigational validation of the BTR-EODLA technique portrayed a superior accuracy value of 98.78% over existing models.

Keywords Brain tumor recognition, Magnetic resonance imaging, Equilibrium optimizer, Image processing, Median filtering, Stacked auto encoder

BT refers to the abnormal growth of cells in the human brain. A tumour that takes place inside the spinal cord or brain is known as a glioma, and the cancer that appears from the meninges is termed a meningioma[1]. The unusual cell development in the pituitary gland is identified as pituitary cancer. The MRI is utilized to recognize and localize the BT. Based on colour contrast transformations, it can also distinguish between oedema, brain tissue, and cerebrospinal fluid[2]. The initial stage of BT recognition is necessary for efficient treatment. Through medical image analysis, the images are attained with several imaging modalities[3]. However, MRI and Computer Tomography (CT) are the dual modalities commonly employed to mark the irregularities based on the size, location, or shape of brain tissues that can assist in identifying cancer; MRI is highly recommended by medical professionals[4]. Consequently, researchers and scientists are more concentrated on MRI. While detecting BCs from MRI images, conventional doctor check-ups are generally used. On the other hand, automatic

[1]Information Technology Department, Faculty of Computing and Information Technology, King Abdulaziz University, Jeddah 21589, Saudi Arabia. [2]Department of Computer Science, Faculty of Computing and Information Technology, King Abdulaziz University, Jeddah 21589, Saudi Arabia. [3] Department of Information Technology, Faculty of Computing and Information Technology, King Abdulaziz University, Rabigh 25732, Saudi Arabia. [4]Biological Sciences Department, College of Science, King Abdulaziz University, Jeddah 21589, Saudi Arabia. [5]Computer and Information Technology Department, The Applied College, King Abdulaziz University, Jeddah 21589, Saudi Arabia. [6]Department of Radiological Sciences, Faculty of Applied Medical Sciences, King Abdulaziz University, Jeddah 21589, Saudi Arabia. [7]King Fahd Medical Research Center, Smart Medical Imaging Research Group , King Abdulaziz University, Jeddah 21589, Saudi Arabia. ✉email: mragab@kau.edu.sa

methodologies mostly executed by computer-aided medical image processing methods are gradually assisting doctors in identifying BC[5]. Automated BT detection and classification procedures are required to decrease the diagnostic time and resolve human mistakes before making some decisions. Recent advancements in ML, particularly in DL, have led to the ability to recognize and categorize medical imaging patterns[6].

Achievements in that domain contain the chance to retrieve and extract data from information instead of learning from professionals or technical texts. ML has rapidly emerged as a supportive tool for improving performance in several medical areas in distinct fields, including prognosis and disease diagnosis, detection of molecular and cellular designs, classification of images, and tissue segmentation[7]. The highly efficient approaches currently used in image processing are Convolutional Neural Networks (CNNs), as they have various layers and enormous analytic precision if the input image quantity is superior. Autoencoders (AEs) are an unsupervised learning method using NNs for representation learning. In addition, numerous ML and DL methods have been used to detect cancer and identify cardiovascular stenosis[8]. In addition, performance evaluations have displayed that they have high diagnosis precision. Early and precise detection of BTs enhances patient outcomes and treatment efficacy. As BTs can substantially impact neurological function, timely diagnosis allows prompt intervention[9]. Advancements in medical imaging technologies have made it possible to capture detailed brain scans, yet interpreting these images remains a threat. By harnessing DL models, the analysis of MRI scans is improved, enabling more precise detection and classification of tumours. This study aims to employ innovative methods to streamline the diagnostic process, ultimately contributing to improved clinical decision-making and patient care[10].

This study presents Brain Tumor Recognition using an Equilibrium Optimizer with a Deep Learning Approach (BTR-EODLA) technique for MRI images. The BTR-EODLA technique intends to recognize whether or not a BT presence exists. In the BTR-EODLA technique, median filtering (MF) eliminates the noise in the input MRI. Besides, the squeeze-excitation ResNet (SE-ResNet50) model is used to derive feature vectors, and its parameters are fine-tuned by the design of the EO model. The BTR-EODLA technique employs the stacked autoencoder (SAE) model for BT detection. A sequence of experiments is performed to ensure the improved performance of the BTR-EODLA technique. The key contribution of the BTR-EODLA technique is listed below.

- A novel MF method is presented to effectively mitigate noise in MRI inputs, improving the clarity of the image. This methodology substantially enhances the quality of the data utilized for subsequent evaluation. Optimizing the input lays the foundation for more precise feature extraction and tumour detection.
- The BTR-EODLA approach employs the SE-ResNet50 method to improve feature vector extraction from MRI data. This advanced architecture enables the technique to concentrate on relevant features, enhancing the evaluation's accuracy. By implementing this method, the study attains enhanced accomplishment in detecting BTs.
- The BTR-EODLA technique fine-tuned parameters by utilizing the EO model, which improved the method's overall performance. This optimization methodology confirms that the model operates at its highest effectiveness, resulting in enhanced accuracy in tumour detection. The strategic adjustment of parameters plays a significant role in attaining reliable outcomes from the MRI analysis.
- An SAE method is employed to attain accurate BT detection from MRI scans. This methodology efficiently captures intrinsic patterns and features relevant to tumour detection. The study improves diagnostic accuracy and reliability in medical imaging by constructing the model for this specific application.
- The incorporation of MF with advanced neural network models presents a unique methodology for MRI analysis and BT detection. This integration not only improves the quality of the image by reducing noise but also enhances the technique's capability to extract critical features. The novel synergy of these approaches allows for more precise and reliable tumour detection, pushing the boundaries of present diagnostic capabilities in medical imaging.

Related works

Mohanty et al.[11] examined a distinct DL methodology that connects the control of a soft-attention device. The technique uses an exactly intended CNN method, including four convolution layers. This technique collects and unites features from every layer. The combination of a soft-attention device at the fatal phases certifies that the clinical and related features were highlighted, improving identification accuracy. Ruba et al.[12] projected a new technique, which segments cancer from 3-D MRI data covering Higher Grade Glioma (HGG). In TLN, 3D-UNet is mainly employed to restrict cancer. Next, intra-tumour areas are segmented utilizing deep CNNs with the developed new operator that depends on LSIS. In[13], a BT recognition and identification method are projected. The developed technique contains five steps. Initially, a linear contrast extension is employed to determine the edges in the source imagery. Next, a custom 17-layered DNN structure has been projected for segmentation. Then, an improved MobileNetV2 structure is employed for the feature extractor and trained to utilize the transfer learning (TL) model. In 4th step, an entropy-based controlled technique was utilized beside a multiclass SVM (M-SVM) for the finest feature selection (FS). Finally, M-SVM was exploited to identify BT.

Agarwal et al.[14] projected the Tumor Detector and Classifier, as well as Auto Contrast Enhancer, to deliver on-demand contrast development of worst contrast MRI imageries. The classifiers achieve their task over a dual-phase model. Throughout the early stage, ODTWCHE improves image contrast, enabling precise analysis of BT. Next, the classifier influences the control of deep TL, using the pre-trained InceptionV3 technique to enhance the analytic procedure and classification of tumours. In[15], a new united end-wise DL technique called TumorDetNet is developed for BT recognition and identification. The TumorDetNet structure uses 48 convolutional layers with leaky ReLU (LReLU) and activation functions of ReLU to calculate the distinct deep feature mappings. Furthermore, a dropout layer and average pooling were utilized to learn different designs and decrease overfitting. Lastly, one FC and softmax layer detects and classifies the BT into manifold kinds. Lamba

et al.[16] presented a new combined method with innovative sub-sets of AI, with DL and supervised learning methods. The projected method utilizes data augmentation to improve the image dimensions and uphold regularization. Next, the technique uses VGG16 layers. Also, the process removes the most major feature and increases the analytic accuracy and speed by utilizing a supervised learning model and linear SVM.

Vaiyapuri et al.[17] project an Ensemble Learning Driven CAD Method for BT Classification (ELCAD-BTC) methodology on MRI. The offered model covers a Gabor Filtering (GF) technique for eliminating the sound and upsurging the excellence of MRI imageries. Furthermore, ensemble learning (EL) of 3 DL techniques, such as DenseNet, MobileNet, and EfficientNet, was exploited as a feature extractor. Besides, the denoising autoencoder (DAE) technique is developed to distinguish the existence of BT. Eventually, the social spider optimizer algorithm (SSOA) is used to parameterize DL approaches. Bose and Garg[18] introduce the Manta Ray Foraging Optimized CNN (MRFO-CNN) approach for classifying brain MRIs into tumorous and non-tumorous categories, utilizing MRFO to optimize hyperparameters like batch size and epochs. Jauro et al.[19] proposes a Symbiotic Organism Search optimization to evolve CNN architectures (SOS_ConvNet) for diverse image classification tasks. Radhika and Mahajan[20] improve the contrast of cardiac MRI images by utilizing the Cetacean Optimization Algorithm (COA) for enhanced disease diagnosis. Rawat and Kumar[21] proposes a hybrid approach that utilizes the Self-Adaptive Jaya Optimization Algorithm (SAJOA) to optimize CNN learning parameters, improving the segmentation of abnormal cells and avoiding local minima.

Several methods for brain tumour detection illustrate specific limitations. One methodology that employs a soft-attention mechanism may encounter enhanced computational complexity, resulting in longer training times and needing extensive labelled data. Another model that depends on 3D MRI data could be less applicable in environments where only 2D scans are available, and its segmentation efficiency may vary across tumour kinds. Furthermore, approaches utilizing linear contrast enhancement risk introducing artefacts that could compromise segmentation accuracy. While dual-phase techniques can improve workflow, their complexity may hinder real-time applications. Large convolutional architectures may increase the risk of overfitting and require substantial computational resources, complicating interpretation. Moreover, integrating DL with supervised approaches necessitates extensive labelled datasets, which are primarily challenging to attain. Lastly, EL models, despite their potential for enhanced accuracy, increase computational demands, and the effectiveness of specific noise reduction techniques may be inconsistent across diverse imaging conditions. Despite improvements in DL models for brain tumour detection, there still needs to be a substantial gap in incorporating noise reduction methods with feature extraction approaches that improve diagnostic accuracy across varying imaging modalities. Additionally, many existing techniques lack robustness when applied to various datasets, emphasizing a need for more adaptable and generalizable methods in clinical settings. More comprehensive datasets encompassing diverse imaging modalities and patient demographics are also needed to improve the generalizability of BT detection models. Also, integrating advanced noise reduction models with feature extraction and classification methods still needs to be explored, limiting the potential for improved diagnostic accuracy in varying clinical scenarios.

Methodology

This paper presents a novel BTR-EODLA methodology for MRI Images. The technique intends to recognize whether BT is present or not. To accomplish that, it comprises image preprocessing, SEan -ResNet50-based feature extractor, EO-based parameter tuning, and SAE-based BT recognition processes, as demonstrated in Fig. 1.

Noise reduction using MF model

Primarily, the BTR-EODLA technique undergoes the MF model and is utilized to eliminate the noise in the input MRI[22]. The selection of the MF model for noise reduction in MRI scans is justified by its efficiency in conserving significant image details while eliminating unwanted noise. Unlike conventional averaging methods, which can blur crucial edges and features, the MF model concentrates on median values, confirming that outliers do not distort the overall image quality. This is advantageous in medical imaging, where precise delineation of anatomical structures is crucial. Furthermore, the MF method outperforms in scenarios with salt-and-pepper noise, a common artefact in MRI images, making it highly appropriate for this application. Its capability to maintain sharp edges while smoothing out noise results in clearer images, improving the accuracy of subsequent analyses and interpretations. Overall, the MF model presents a balanced methodology, effectually addressing noise while retaining the integrity of critical features in the imaging data. Figure 2 illustrates the structure of the MF model.

The MF model is a digital image processing algorithm that removes noise from the image while maintaining its essential details and edges. The MF model replaces all the pixels with the median value from its neighbourhood, which is different from the classical MF model, which replaces all the pixels with the average of the adjacent pixels. This technique is highly successful in scenarios where the images have salt-and-pepper noise (dark and bright pixels). By choosing the median values, noise (outliers) is successfully removed, leading to a smoother image without significantly blurring sharp edges or transitions.

Feature extraction

Next, the SE-ResNet50 method derives feature vectors[23]. The SE-ResNet50 method was selected for deriving feature vectors due to its enhanced architecture that efficiently captures intrinsic patterns in MRI data. Its SE mechanism allows for dynamic channel-wise feature recalibration, improving the technique's capability to concentrate on the most relevant features while suppressing less informative ones. This results in enhanced performance in tasks such as brain tumour detection, where precise feature extraction is significant. Furthermore, ResNet's skip connections facilitate effectual training and reduce such problems as vanishing gradients, enabling

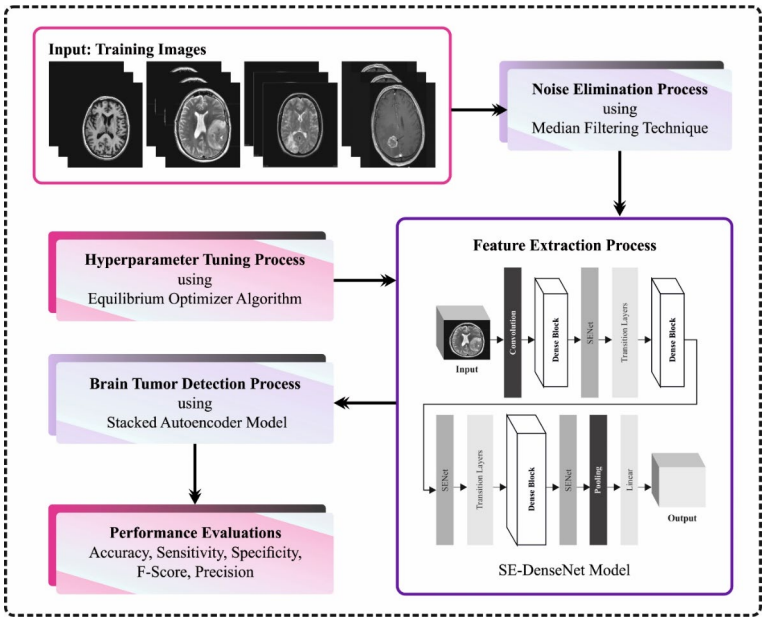

Fig. 1. Workflow of BTR-EODLA technique.

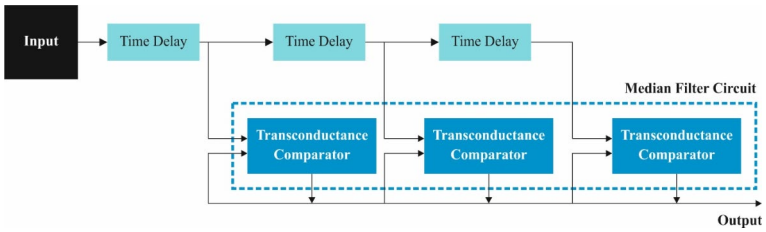

Fig. 2. Structure of MF model.

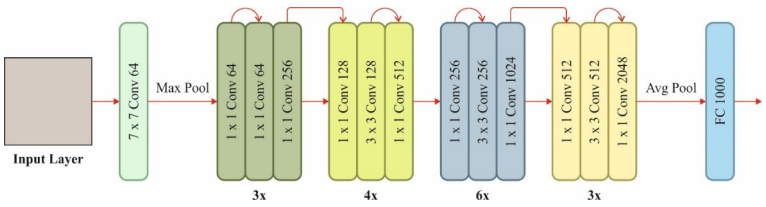

Fig. 3. Architecture of ResNet-50 technique.

deeper architectures without compromising performance. Integrating depth and SE blocks in the ResNet50 framework confirms that the model learns richer feature representations and maintains robustness across diverse imaging conditions, making it a greater choice than conventional CNNs models. Figure 3 demonstrates the architecture of the ResNet-50 methodology.

This work picks ResNet-50, a deep neural network (DNN) based on residual learning, as the vital method for forecasting complex tastes. ResNet certifies the transmission of data across many hidden layers (HLs) by inserting skip connections among convolution (Conv) layers, efficiently improving the problems of gradient loss and network degradation existing in conventional DNN and allowing the system to grow to many layers. Since the method's performance and parameters are comprehensive, ResNet-50 was selected as the simple network structure in this work.

The ResNet-50 structure contains five sets of Conv layers (a complete 49 Conv layers) and one FC layer. After a 7x7 Conv and 3×3 max-pooling layers, the output feature dimension is decreased by a semi. In the following four sets, Conv kernels of dimensions 1×1 and 3×3, are correspondingly employed to remove features of dissimilar dimensions from the images, with the activation function of ReLU after the Conv layers. This structure decreases the method parameters and computation workload, whereas 1×1 Conv kernels upsurge the network

depth and improve the system's nonlinearity. The output dimensional of the last FC layer relates to the integer of taste molecule classes.

This module is a feature fusion model for improving the CNN performance. It pretends the mechanism of human attention, permitting the method to concentrate more on significant channel data and overwhelm less significant channel features, thereby refining the system's classification efficacy. At first, the input feature i of every channel C is generally pooled and averaged in spatial dimension through the compression process F_{sq}. Then, the pooled features are served into dual FC layers utilizing the excitation process F_{ex}, whereas the initial FC layer employs ReLU, and the next FC layer utilizes the sigmoid function to obtain the weight value for every feature channel. Lastly, the weight values are used to achieve the element-wise scaling process F_{scole} on the novel features and re-calibrate them to attain the removed attention feature. The formulations for calculating F_{sq}, F_{ex}, and F_{scole} are given below.

$$Z_c = \rho_{sq}\left(u_c\right) = \frac{1}{H \times W}\sum_{j=1}^{H}\sum_{j=1}^{W} u_c\left(i, j\right) \tag{1}$$

$$S = F_{ex}\left(z, W\right) = \sigma\left(W_2\delta\left(W_1 z\right)\right) \tag{2}$$

$$\tilde{o}_c = F_{scole}\left(u_c, s_c\right) = s_c \bullet u_c \tag{3}$$

whereas $u_c(i, j)$ signifies the feature value of channel C at location (i, j), W_1 and W_2 refer to the weight values of dual FC layers. δ and σ represent the activation functions of ReLU and Sigmoid, correspondingly.

EO-based hyperparameter tuning

At this stage, the EO approach's design adjusts the hyperparameters[24]. The EO method is selected for hyperparameter adjustment due to its robust and effectual optimization capabilities. Unlike conventional optimization models, EO is inspired by the principles of equilibrium in nature, allowing it to navigate intrinsic solution spaces more efficiently. This results in an enhanced convergence rates and the capability to escape local minima, which is significant for improving the performance of the model in tasks like brain tumor detection. The EO method also needs lesser hyperparameter tuning iterations, saving both time and computational resources. Furthermore, its flexibility makes it appropriate for a variety of model architectures, confirming adaptability across diverse scenarios and datasets. By employing EO for hyperparameter adjustment, more accurate and reliable models can be attained that are better equipped to handle the complexities of medical imaging data.

The EO approach determines the problem solution in an effective and efficient method with the exploitation and exploration search stages. The EO methodology is a physics-based method stimulated by the demonstration of dynamic mass balance performance utilized to investigate the focus on non-reactive modules in control volume production. During this EO technique, the equilibrium state follows once the particles influence the global optimum rate. The steps of the method are provided as:

(1) (1) The optimizer method is derived from expressing the individuals from the searching space during the EO technique. In the procedure, by utilizing Eq. (4), all the particles upgrade their concentration based on the optimum results, which are named equilibrium candidates.

$$C_i^{initial} = C_{\min} + rand_i\left(C_{mox} - C_{\min}\right), i = 1, 2, \ldots, n. \tag{4}$$

$C_i^{initial}$ refers to the primary concentration vector of $thej^{th}$ particle, $C_{\min}$ and $C_{\max}$ stand for the minimal and maximal rates for the sizes, n defines the particle counts from the population, and $rand$ represents the random numbers from zero to one. The determination of particles relies on the rate of the fitness function (FF). Afterwards, they are ranked based on their fitness values.

(2) The EO technique proposes determining the balance model under the procedure. The candidate performances of the method are elected as the 4 optimum particles under the method and their concentrations. The 5th equilibrium particle has been acquired by calculating the arithmetic average of elected particles. Eq. (4) and (5) are employed for creating the vectors of the equilibrium pool.

$$C_{\text{avg}} = \frac{C_{eq1} + C_{eq2} + C_{eq3} + C_{eq4}}{4}. \tag{5}$$

$$C_{eq,pool} = \left\{C_{eq1}, C_{eq2}, C_{eq3}, C_{eq4}, C_{eq(\text{avg})}\right\}. \tag{6}$$

(3) The EO model comprises 2 phases: exploration and exploitation. The four optimum elected candidate performance rates are employed during this exploration step. The capacity of the exploitation step was established by the average rate of 4 computed candidates. The exponential term F recognises the balance among these two steps provided in Eq. (7)

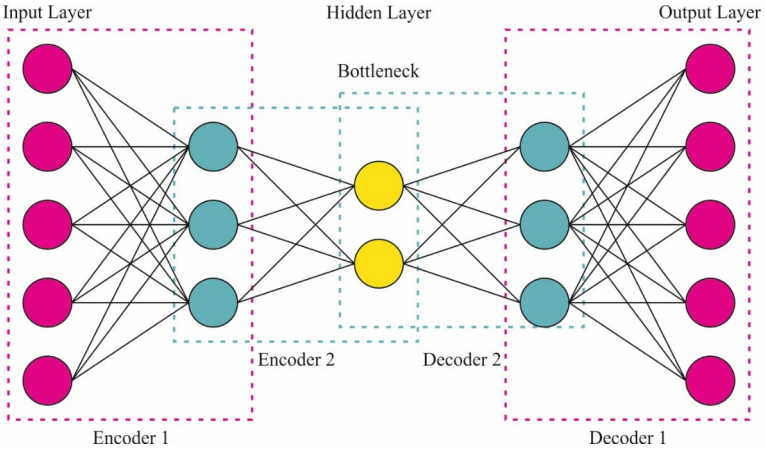

Fig. 4. Architecture of SAE model.

Classes	No. of instances
Tumor	153
No tumor	98
Total instances	251

Table 1. Details of the dataset.

$$\begin{aligned} F &= a_1 sign\,(r-0.5)\left[e^{-\sigma t}-1\right]. \\ t &= \left(1-\frac{iter}{\max\_iter}\right)^{\left(0_2\frac{iter}{maxiter}\right)}. \end{aligned} \tag{7}$$

It is a random vector among σ and $r[0,1]$; the t rate reduces as the iteration counts enhance. $iter$ and $\max\_iter$ signify the present and maximal iteration counts; correspondingly, a_2 denotes the finding ability constant. The superior a_2, the robust the exploration proficiency, and the lesser the exploitability. a_1 rate is the opposite of the occurrence of $thea_2$ variable. The higher the rate of a_2, the more significant the influence on the exploit step. On the other hand, the result is low under the discovery step.

(4) The outcome of production value (G) is a significant part of the exploitation step of the EO method. Equation (8) demonstrates the rate of production.

$$\begin{aligned} G &= G_0 F. \\ G_0 &= GCP\,(C_{eq}-\sigma C). \\ GCP &= \begin{cases} 0.5r_1 & r_2 \geq GP \\ 0 & r_2 \leq GP. \end{cases} \end{aligned} \tag{8}$$

A primary rate G_0 signifies the arbitrarily varying number among r_1 and $r_2[0,1]$, GCP denotes the output coefficient of the production rate, and GP defines the production rate employed from the position upgrade. At last, the common upgrade rule of particle states can be represented by Eq. (9). C and C_{eq} denote the present particle and the equilibrium candidate performances.

$$C = C_{eq} + (C - C_{eq})\,F + \frac{G}{\sigma V}\,(1-F). \tag{9}$$

Fitness choice is a significant factor in controlling the efficiency of the EO approach. Hyperparameter tuning uses the encoding method to measure the solution of candidate outcomes. During this case, the EO method assumes that accuracy is a main condition to design the FF that is expressed as:

$$Fitness = \max\ (P) \tag{10}$$

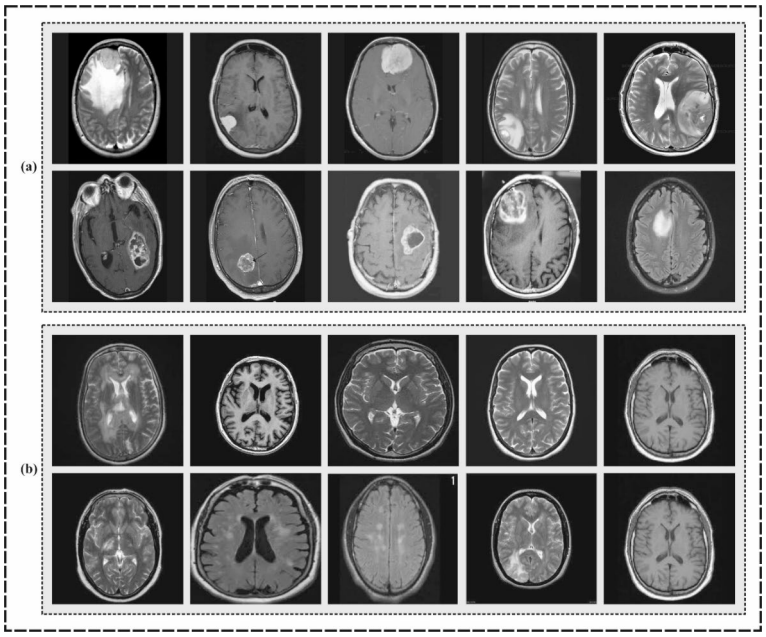

Fig. 5. Sample images (**a**) Tumor and (**b**) No-Tumor.

Sample Image	PSNR (dB)			SSIM		
	MF	BF	SF	MF	BF	SF
Img-1	36.49	24.49	11.49	0.94	0.92	0.87
Img-2	34.11	20.11	10.11	0.93	0.91	0.83
Img-3	34.48	23.48	12.48	0.92	0.90	0.82
Img-4	33.70	20.70	7.70	0.93	0.93	0.87
Img-5	32.88	18.88	8.88	0.93	0.92	0.84
Average	34.33	21.53	10.13	0.93	0.92	0.85

Table 2. Analysis of various filtering techniques on applied dataset using PSNR and SSIM.

$$P = \frac{TP}{TP + FP} \tag{11}$$

whereas FP and TP illustrate the false and true positive rates.

BT Detection using the SAE model

For BT detection, the BTR-EODLA technique exploits the SAE model[25]. This technique is chosen due to its capability to learn hierarchical feature representations from intrinsic MRI data effectually. Unlike conventional methods, SAEs can capture complex patterns and relationships within the data by progressively mitigating dimensionality, making them specifically appropriate for medical imaging applications. This unsupervised learning model allows the approach to detect relevant features without extensive labeling, which is mostly a threat in medical datasets. Furthermore, the capacity of the SAE model to reconstruct input data improves its robustness against noise and artifacts, common in MRI scans. By employing this approach, the accuracy and reliability of tumor detection can be improved while minimizing the risk of overfitting that can occur with deeper supervised networks. Overall, the SAE method presents a balanced approach, incorporating effectual feature extraction with a flexible architecture tailored for complex medical imaging tasks. Figure 4 represents the structure of SAE method.

The AE architecture includes an encoding and a decoding part. The encoder reduces the data dimensionality and extracts the input data features. The decoder recreates new data from the extracted features. The encoder is adopted in the training to map the input $X \in R^h$ to the low-level representation $Y \in R^i$, and the decoder is used to recover $\tilde{X} \in R^h$ from $Y \in R^i$. The training diminishes the error between X and $\tilde{X}$.

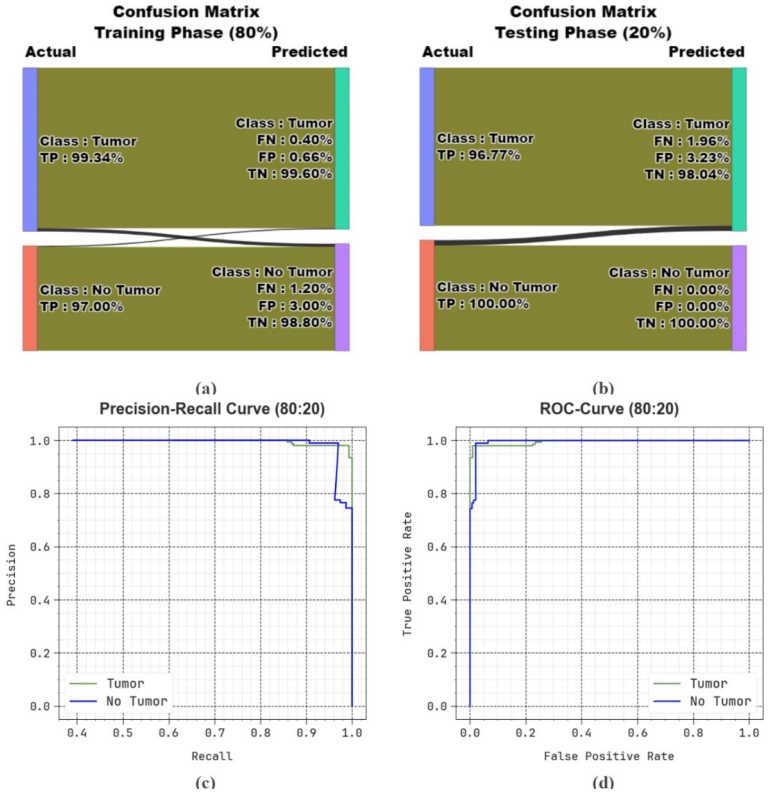

Fig. 6. 80%TRP and 20%TSP of (**a**, **b**) Confusion matrices and (**c**, **d**) PR and ROC curves.

Class	$Accu_y$	$Prec_n$	$Sens_y$	$Spec_y$	F_{Score}
TRP (80%)					
Tumor	97.56	100.00	97.56	100.00	98.77
No Tumor	100.00	96.25	100.00	97.56	98.09
Average	98.78	98.12	98.78	98.78	98.43
TSP (20%)					
Tumor	100.00	96.77	100.00	95.24	98.36
No Tumor	95.24	100.00	95.24	100.00	97.56
Average	97.62	98.39	97.62	97.62	97.96

Table 3. Recognition outcome of BTR-EODLA technique at 80%TRP and 20%TSP.

$$\begin{aligned} Y &= f\left(W_e X + b_e\right) \\ \tilde{X} &= g\left(W_d Y + b_d\right) \\ &\arg\ \text{smin}\ \left[loss\left(X, \tilde{X}\right)\right] \end{aligned} \tag{12}$$

In Eq. (12), W_e, b_e, and $f(\cdot)$ and W_d, b_d, and $g(\cdot)$ are the weights, bias, and activation functions of encoding and decoding, respectively.

The encoder is used during testing to extract features, which are then input into a classifier for classification. The decoder obtains recreated data in the training stage. The data recreated is nearer to the input dataset, considering the feature is more representative.

The encoder and decoder have a multi-layer neural network in AE, known as SAE technique. Generally, the operations of encoding and decoding are inverse, and the operation layers of decoding and encoding are identical. Likewise, the decoding and encoding are symmetrical structures. This makes the construction of the SAE model much easier. Nevertheless, it is challenging to upsurge the depth of the SAE model because once the encoded adds one layer, the decoded should add one layer, making them rise by 2. A structurally asymmetrical SAE approach is introduced to enhance the encoded depth, where the decoder layer is lesser than the encoded. This means there are trainable parameters and multiple layers encoded for extracting features.

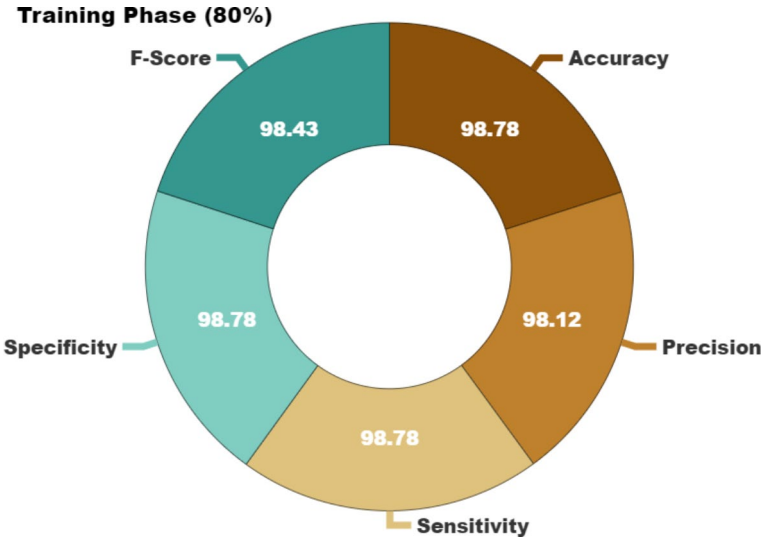

Fig. 7. Average outcome of BTR-EODLA technique at 80%TRP.

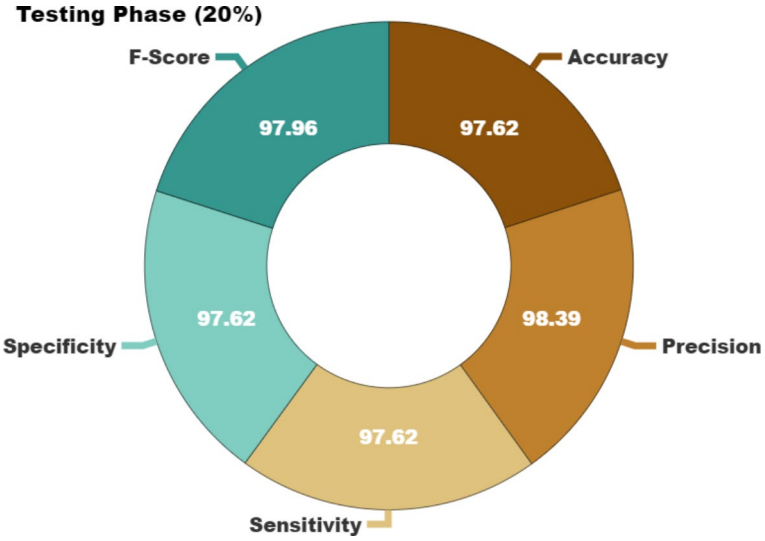

Fig. 8. Average outcome of BTR-EODLA technique at 20%TSP.

Result analysis and discussion

This article studies the performance of the BTR-EODLA methodology on the brain MRI dataset from Kaggle[26]. Table 1 represents the dataset comprising 153 tumours and 98 non-tumour samples. Figure 5 demonstrates the sample images.

Table 2 shows the comparison of the performance of the MF with two other image filtering techniques namely Bilateral Filter (BF) and Sobel Filter (SF), based on PSNR and SSIM metrics across five sample images. The MF consistently outperforms other techniques, achieving the highest PSNR (up to 36.49 dB for Img-1) and SSIM (0.94 for Img-1), with an average PSNR of 34.33 dB and SSIM of 0.93. The BF follows closely, with an average PSNR of 21.53 dB and SSIM of 0.92, while the SF gives the lowest values, with an average PSNR of 10.13 dB and SSIM of 0.85, illustrating its limited effectualness in conserving image quality. Overall, the MF gives an optimum balance of quality enhancement, with the BF presenting a reasonable alternative, while the SF shows the least improvement in both metrics.

Figure 6 shows the classifier outcomes of the BTR-EODLA model at 80%TRP and 20%TSP. Figures 6a, b illustrates the confusion matrices produced by the BTR-EODLA model. The result was that the BTR-EODLA method recognized and categorized two classes. Then, Fig. 6c describes the PR analysis of the BTR-EODLA method. The experimental values showed that the BTR-EODLA methodology acquired a higher PR value in 2 classes. However, Fig. 6d represents the ROC investigation of the BTR-EODLA methodology. The experimental values depicted that the BTR-EODLA model resulted in proficient performances with better outcomes of ROC at two classes.

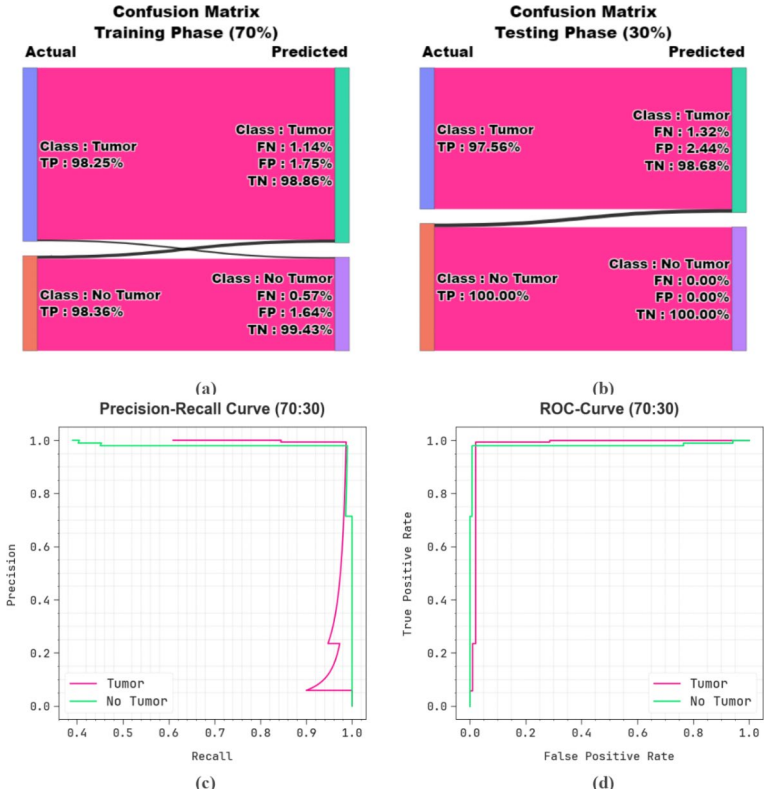

Fig. 9. 70%TRP and 30%TSP of (**a**, **b**) Confusion matrices and (**c**, **d**) PR and ROC curves.

Class	$Accu_y$	$Prec_n$	$Sens_y$	$Spec_y$	F_{Score}
TRP (70%)					
Tumor	99.12	98.25	99.12	96.77	98.68
No Tumor	96.77	98.36	96.77	99.12	97.56
Average	97.94	98.30	97.94	97.94	98.12
TSP (30%)					
Tumor	100.00	97.56	100.00	97.22	98.77
No Tumor	97.22	100.00	97.22	100.00	98.59
Average	98.61	98.78	98.61	98.61	98.68

Table 4. Recognition outcome of BTR-EODLA methodology at 70%TRP and 30%TSP.

Table 3 presents a brief recognition of the BTR-EODLA methodology's results for 80%TRP and 20%TSP. The tabulated values infer that the BTR-EODLA methodology proficiently recognizes the tumour samples.

Figure 7 reveals the average detection results of the BTR-EODLA technique on 80%TR7. The experimental values indicate that the BTR-EODLA technique can effectively identify the samples. The BTR-EODLA methodology also reaches average $accu_y$, $prec_n$, $sens_y$, $spec_y$, and F_{score} of 98.78%, 98.12%, 98.78%, 98.78%, and 98.43%, respectively.

The average detection outcomes of the BTR-EODLA methodology on 20%TSP are revealed in Fig. 8. The result implies that the BTR-EODLA methodology can efficaciously recognize the samples. It is also detected that the BTR-EODLA technique gains average $accu_y$, $prec_n$, $sens_y$, $spec_y$, and F_{score} of 97.62%, 98.39%, 97.62%, 97.62%, and 97.96%, correspondingly.

Figure 9 exhibits the classifier outcomes of the BTR-EODLA technique at 70%TRP and 30%TSP. Figure 9a, b shows the confusion matrices attained by the BTR-EODLA technique. The outcome stated that the BTR-EODLA methodology has classified and recognized two classes. Afterwards, Fig. 9c defines the PR outcome of the BTR-EODLA methodology. The experimental result showed that the BTR-EODLA approach attains greater PR values in 2 classes. But, Fig. 9d exemplifies the ROC outcome of the BTR-EODLA approach. The simulation results defined that the BTR-EODLA model has resulted in proficient results with better outcomes of ROC at 2 class labels.

Table 4 depicts a brief recognition outcome of the BTR-EODLA methodology for 70%TRP and 30%TSP. The tabulated outcomes inferred that the BTR-EODLA method proficiently identifies the tumour samples.

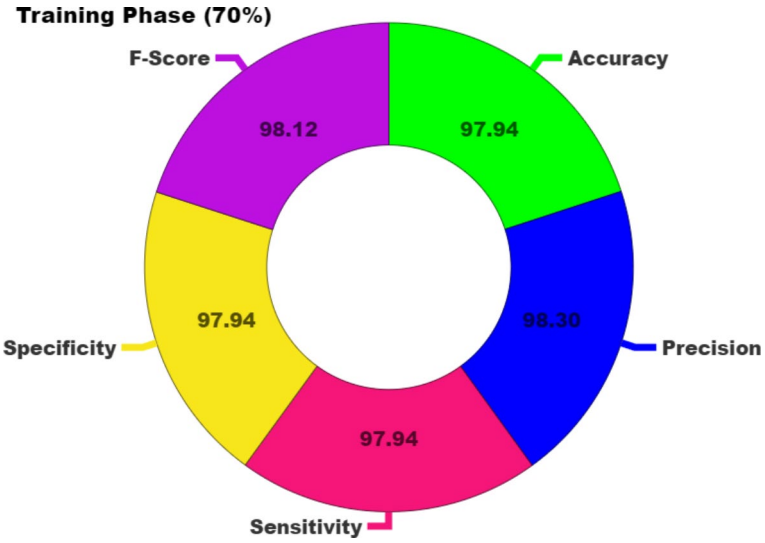

Fig. 10. Average outcome of BTR-EODLA technique at 70%TRP.

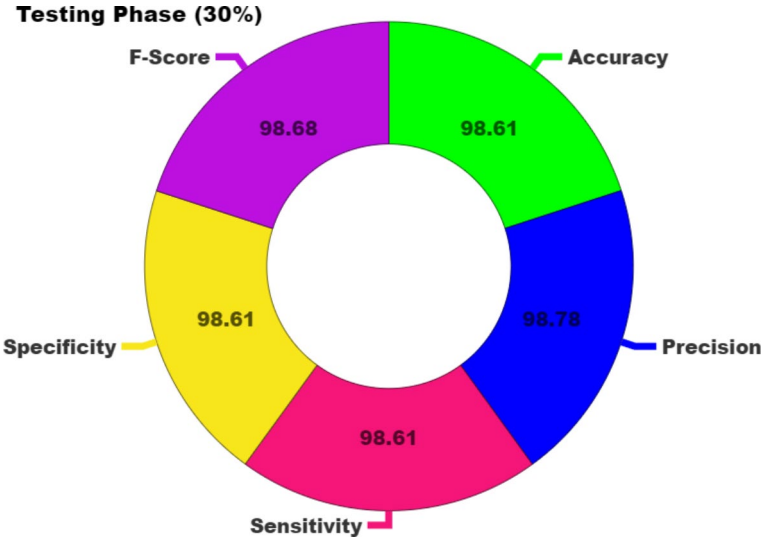

Fig. 11. Average outcome of BTR-EODLA technique at 30%TSP.

Methods	$Accu_y$	$Prec_n$	$Recal_l$	F_{Score}	AUC_{Score}	MCC
DC-FOF	85.60	86.00	89.30	89.20	85.54	93.68
HEC	89.00	90.20	93.00	93.20	88.67	94.54
RBFNN	90.20	91.00	94.50	95.00	97.09	85.03
MENF	92.30	92.30	95.40	96.70	96.47	87.28
RG-FCM-HHOCNN	98.00	97.90	98.07	98.08	87.04	95.62
MRFO-CNN	95.27	97.75	97.53	91.52	89.42	94.18
SOS_ConvNet	96.44	91.41	97.27	97.96	86.82	83.90
COA	89.99	94.63	96.27	95.22	92.14	94.80
SAJOA	95.85	93.23	93.48	91.36	85.31	88.35
BTR-EODLA	98.78	98.12	98.78	98.43	98.11	98.25

Table 5. Comparative outcome of BTR-EODLA technique with recent models.

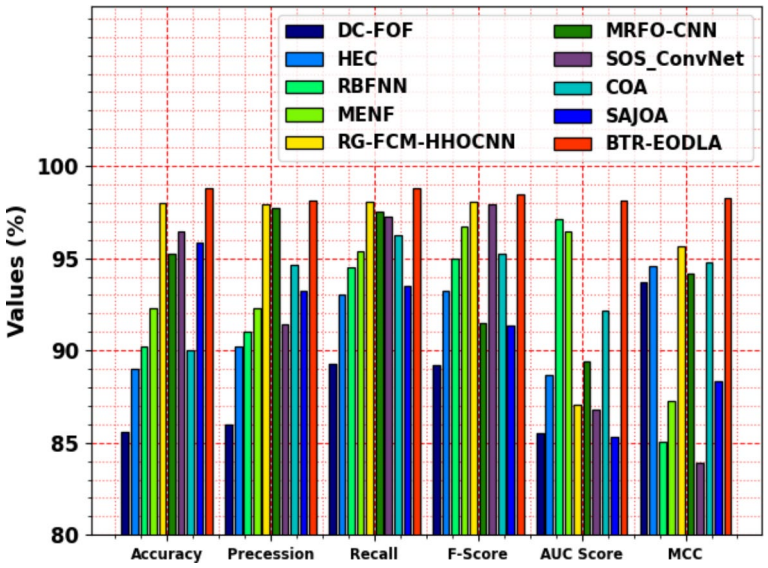

Fig. 12. Comparative outcome of BTR-EODLA technique with recent models.

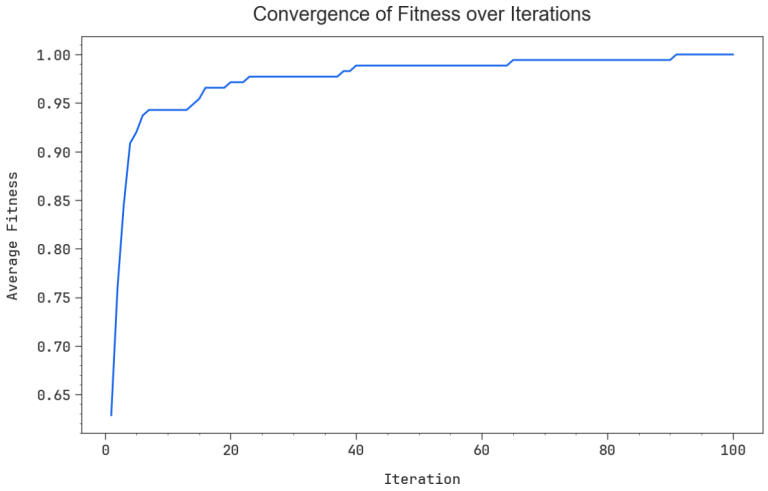

Fig. 13. Convergence of fitness values for the BTR-EODLA model.

Methods	CT (sec)
DC-FOF	19.87
HEC	14.97
RBFNN	19.64
MENF	13.48
RG-FCM-HHOCNN	11.78
MRFO-CNN	18.38
SOS_ConvNet	23.13
COA	19.50
SAJOA	24.08
BTR-EODLA	8.30

Table 6. CT analysis of the BTR-EODLA technique over existing models.

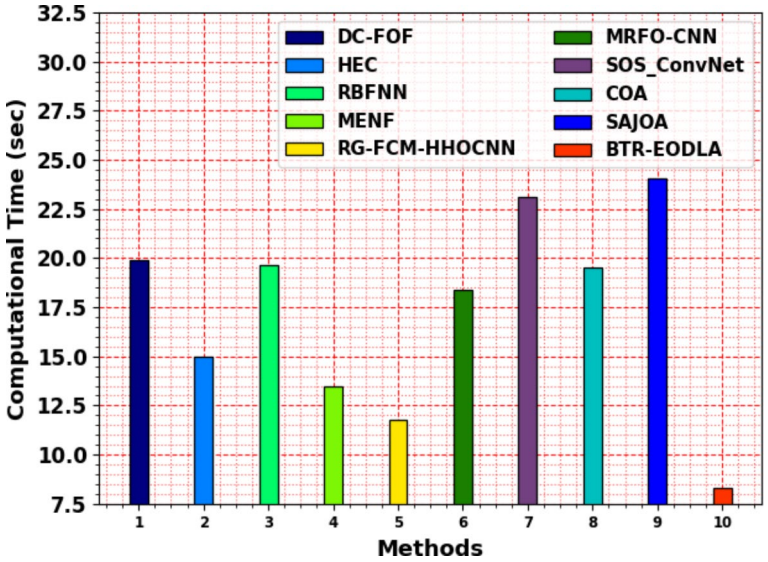

Fig. 14. CT analysis of the BTR-EODLA technique over existing models.

Methods	Accuracy (%)
BTR-EODLA	98.78
SE-DenseNet	97.15
Inception Model	95.35
ResNet-50 Model	93.56
ResNet-101 Model	91.85
VGG19 Model	90.25

Table 7. Ablation analysis of the BTR-EODLA technique over various models.

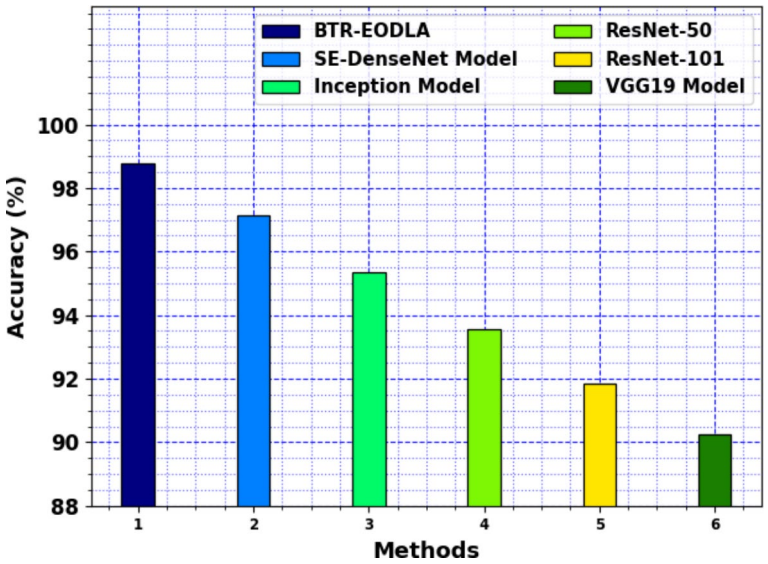

Fig. 15. Ablation analysis of the BTR-EODLA technique over various models.

The average recognition outcome of the BTR-EODLA model on 70%TRP is exemplified in Fig. 10. The experimental values defined that the BTR-EODLA model can effectually recognize the samples. It is also observed that the BTR-EODLA methodology reaches average $accu_y$, $prec_n$, $sens_y$, $spec_y$, and F_{score} of 97.94%, 98.30%, 97.94%, 97.94%, and 98.12%, correspondingly.

The average detection outcomes of the BTR-EODLA approach on 30%TSP are depicted in Fig. 11. The table values state that the BTR-EODLA approach can efficiently identify the samples. It is also noted that the BTR-EODLA methodology achieves average $accu_y$, $prec_n$, $sens_y$, $spec_y$, and F_{score} of 98.61%, 98.78%, 98.61%, 98.61%, and 98.68%, correspondingly.

Table 5 and Fig. 12 depicts the comparison study of the BTR-EODLA model over recent approaches[27]. The results exhibit that the DC-FOF model has shown worse performance with $accu_y$, $prec_n$, $reca_l$, and F_{score} of 85.60%, 86.00%, 89.30%, and 89.20%, respectively. Simultaneously, the HEC method has obtained somewhat increased outcomes with $accu_y$, $prec_n$, $reca_l$, and F_{score} of 89.00%, 90.20%, 93.00%, and 93.20%, respectively. Besides, the RBFNN and MENF models have attained moderately closer performance. Meanwhile, the RG-FCM-HHOCNN model has resulted in considerable outcomes with $accu_y$, $prec_n$, $reca_l$, and F_{score} of 98.00%, 97.90%, 98.07%, and 98.08%, respectively.

But the BTR-EODLA technique outperforms the other models with maximum $accu_y$, $prec_n$, $reca_l$, and F_{score} of 98.78%, 98.12%, 98.78%, and 98.43%, respectively. Therefore, the BTR-EODLA technique is applied to the automated BT recognition process.

Figure 13 depicts the convergence of fitness values over iterations, demonstrating the optimization process and improvement in performance across the first 100 iterations. Initially, the fitness values start at a lower level but gradually increase, attaining a peak before stabilizing. This behavior reflects the optimization process, where the approach refines its solutions over time, ultimately attaining a high fitness value by the 100th iteration.

Table 6 and Fig. 14 illustrates the computational time (CT) analysis of the BTR-EODLA model over existing techniques. The CT (in seconds) for several methods are as follows: DC-FOF takes 19.87 s, HEC requires 14.97 s, RBFNN takes 19.64 s, and MENF completes in 13.48 s. RG-FCM-HHOCNN operates in 11.78 s, while MRFO-CNN takes 18.38 s. SOS_ConvNet has a longer processing time of 23.13 s, and COA requires 19.50 s. SAJOA is the slowest with a time of 24.08 s, whereas the BTR-EODLA method demonstrates the fastest performance at just 8.30 s.

Table 7 and Fig. 15 shows the ablation study of the BTR-EODLA approach under diverse models. The ablation study evaluates the performance of the proposed BTR-EODLA method in comparison with several well-established models in terms of classification accuracy. The BTR-EODLA method attained the greatest accuracy of 98.78%, setting a benchmark in the performance for the task. In comparison, SE-DenseNet followed with an accuracy of 97.15%, indicating strong performance, but slightly lesser than the BTR-EODLA model. Other widely used models such as Inception, ResNet-50, and ResNet-101 performed with accuracies of 95.35%, 93.56%, and 91.85%, respectively, exhibiting their proficiency but underscoring a notable gap when related to BTR-EODLA model. The traditional VGG19 model, while still widely used, had the lowest accuracy in this study at 90.25%, suggesting that while effective, it may not be the most suitable choice for the given task. This elaborated ablation study emphasizes the superior performance of the BTR-EODLA model over existing techniques, showing its potential in achieving higher accuracy for the classification task.

Conclusion

In this paper, a novel BTR-EODLA technique on MRI Images is presented. The BTR-EODLA technique intends to recognize whether or not a BT presence exists. The BTR-EODLA technique encompasses image preprocessing, SE-ResNet50-based feature extractor, EO-based parameter tuning, and SAE-based BT recognition processes to accomplish that. Primarily, the BTR-EODLA technique undergoes the MF, eliminating the noise in the input MRI. Besides, the SE-ResNet50 model is utilized to derive feature vectors, and its parameters are fine-tuned by the EO model's design. For BT detection, the BTR-EODLA technique implements the SAE approach. A sequence of experiments is performed to ensure the improved performance of the BTR-EODLA technique. The simulation outcomes ensured that the BTR-EODLA technique gains improved performance over other models. The investigational validation of the BTR-EODLA technique portrayed a superior accuracy value of 98.78% over existing models. The limitations of the existing studies encompass a reliance on relatively small and heterogeneous datasets, which may deter the generalizability of the models developed. Many models also need help to overfit due to the high complexity of DL models when trained on limited samples. Furthermore, more real-time applicability in clinical settings poses a crucial threat, as most methods need extensive preprocessing and computation. Future studies should concentrate on expanding datasets to comprise a wide range of tumour kinds and imaging conditions, enhancing the robustness and adaptability of the model. Integrating TL and data augmentation methods could also improve the model's performance. Moreover, developing lightweight models appropriate for deployment in real-time clinical environments will be crucial for translating these methods into practical use. Lastly, collaborative efforts to create standardized datasets ease improved benchmarking and comparison across studies.

Data availability

The datasets used and analyzed during the current study available from the corresponding author on reasonable request.

Received: 11 July 2024; Accepted: 22 November 2024
Published online: 27 November 2024

References

1. Benbakreti, S., Benouis, M., Roumane, A. & Benbakreti, S. Impact of the data augmentation on the detection of brain tumor from MRI images based on CNN and pretrained models. *Multimed. Tools Appl.* **83**(13), 39459–39478 (2024).
2. Rajendran, S. et al. Automated segmentation of brain tumor MRI images using deep learning. *IEEE Access* **11**, 64758–64768 (2023).
3. Khan, M. S. I. et al. Accurate brain tumor detection using deep convolutional neural network. *Comput. Struct. Biotechnol. J.* **20**, 4733–4745 (2022).
4. Cekic, E., Pinar, E., Pinar, M. & Dagcinar, A. Deep learning-assisted segmentation and classification of brain tumor types on magnetic resonance and surgical microscope images. *World Neurosurg.* **182**, e196–e204 (2024).
5. Asad, R. et al. Computer-aided early melanoma brain-tumor detection using deep-learning approach. *Biomedicines* **11**(1), 184 (2023).
6. Batool, A. & Byun, Y. C. Brain tumor detection with integrating traditional and computational intelligence approaches across diverse imaging modalities-challenges and future directions. *Comput. Biol. Med.* 108412 (2024).
7. Mandle, A. K., Sahu, S. P. & Gupta, G. P. CNN-based deep learning technique for the brain tumor identification and classification in MRI images. *Int. J. Softw. Sci. Comput. Intell.* **14**(1), 1–20 (2022).
8. Kanchanamala, P., Revathi, K. G. & Ananth, M. B. J. Optimization-enabled hybrid deep learning for brain tumor detection and classification from MRI. *Biomed. Signal Process. Control* **84**, 104955 (2023).
9. Nassar, S. E., Yasser, I., Amer, H. M. & Mohamed, M. A. A robust MRI-based brain tumor classification via a hybrid deep learning technique. *J. Supercomput.* **80**(2), 2403–2427 (2024).
10. Rasheed, Z. et al. Automated classification of brain tumors from magnetic resonance imaging using deep learning. *Brain Sci.* **13**(4), 602 (2023).
11. Mohanty, B. C., Subudhi, P. K., Dash, R. & Mohanty, B. Feature-enhanced deep learning technique with soft attention for MRI-based brain tumor classification. *Int. J. Inf. Technol.* 1–10 (2024).
12. Ruba, T., Tamilselvi, R. & Beham, M. P. Brain tumor segmentation in multimodal MRI images using novel LSIS operator and deep learning. *J. Amb. Intell. Human. Comput.* **14**(10), 13163–13177 (2023).
13. Maqsood, S., Damaševičius, R. & Maskeliūnas, R. Multi-modal brain tumor detection using deep neural network and multiclass SVM. *Medicina* **58**(8), 1090 (2022).
14. Agarwal, M. et al. Deep learning for enhanced brain tumor detection and classification. *Results Eng.* **22**, 102117 (2024).
15. Ullah, N. et al. TumorDetNet: A unified deep learning model for brain tumor detection and classification. *Plos One* **18**(9), e0291200 (2023).
16. Lamba, K., Rani, S., Anand, M. & Maguluri, L. P. An integrated deep learning and supervised learning approach for early detection of brain tumor using magnetic resonance imaging. *Healthcare Analyt.* **5**, 100336 (2024).
17. Vaiyapuri, T., Jaiganesh, M., Ahmad, S., Abdeljaber, H. A., Yang, E. & Jeong, S. Y. Ensemble learning driven computer-aided diagnosis model for brain tumor classification on magnetic resonance imaging. *IEEE Access*. (2023).
18. Bose, A. & Garg, R. Optimized CNN using manta-ray foraging optimization for brain tumour detection. *Proc. Comput. Sci.* **235**, 2187–2195 (2024).
19. Jauro, F. et al. Modified symbiotic organisms search optimization for automatic construction of convolutional neural network architectures. *Intell. Syst. Appl.* **22**, 200349 (2024).
20. Radhika, R. & Mahajan, R. Cetacean optimization based medical image contrast-enhancement technique for improving disease diagnosis in cardiac MRI. *Proc. Comput. Sci.* **235**, 1615–1622 (2024).
21. Rawat, A. & Kumar, R. A hybrid DL architecture for improved generalizability with self-adaptive jaya optimizer for diabetic retinopathy. *Proc. Comput. Sci.* **235**, 2090–2100 (2024).
22. Shah, A. et al. Comparative analysis of median filter and its variants for removal of impulse noise from gray scale images. *J. King Saud Univ. Comput. Inf. Sci.* **34**(3), 505–519 (2022).
23. Lin, F., Ji, Y. & Xu, S. Sweetener identification using transfer learning and attention mechanism. *CyTA J. Food* **22**(1), 2341812 (2024).
24. Atban, F., Ekinci, E. & Garip, Z. Traditional machine learning algorithms for breast cancer image classification with optimized deep features. *Biomed. Signal Process. Control* **81**, 104534 (2023).
25. Bai, Y., Sun, X., Ji, Y., Fu, W. & Zhang, J. Two-stage multi-dimensional convolutional stacked autoencoder network model for hyperspectral images classification. *Multimed. Tools Appl.* **83**(8), 23489–23508 (2024).
26. https://www.kaggle.com/datasets/navoneel/brain-mri-images-for-brain-tumor-detection
27. Kurdi, S. Z. et al. Brain tumor classification using meta-heuristic optimized convolutional neural networks. *J. Personal. Med.* **13**(2), 181 (2023).

Acknowledgements

This Project was funded by the Deanship of Scientific Research (DSR) at King Abdulaziz University (KAU), Jeddah, Saudi Arabia, under grant no. (GPIP-245-611-2024). Therefore, the authors acknowledge DSR at KAU for technical and financial support.

Author contributions

Conceptualization: Mahmoud Ragab, Iyad Katib; Data curation and Formal analysis: Hassan A. Alterazi, Sanaa A. Sharaf; Investigation and Methodology: Sana G. Alattas, Jaber Alyami; Project administration and Resources: Mahmoud Ragab; Validation and Visualization: Sami Saeed Binyamin, Alanoud Subahi; Writing—original draft, Mahmoud Ragab, Iyad Katib, Sanaa A. Sharaf, Hassan A. Alteraz; Writing—review and editing, Jaber Alyami, Sami Saeed Binyamin, Alanoud Subahi, Sana G. Alattas. All authors have read and agreed to the published version of the manuscript.

Declarations

Competing interests

The authors declare that they have no conflict of interest. The manuscript was written with the contributions of all authors. All authors have approved the final version of the manuscript.

Additional information

Correspondence and requests for materials should be addressed to M.R.